J. Am. Soc. Mass Spectrom. (2017) 28:1333–1344
DOI: 10.1007/s13361-016-1586-7

FOCUS: BIO-ION CHEMISTRY: INTERACTIONS OF BIOLOGICAL IONS WITH IONS, MOLECULES, SURFACES, ELECTRONS, AND LIGHT : RESEARCH ARTICLE

Near-UV Photodissociation of Tryptic Peptide Cation Radicals. Scope and Effects of Amino Acid Residues and Radical Sites

Huong T. H. Nguyen, František Tureček

Department of Chemistry, University of Washington, Bagley Hall, Box 351700, Seattle, WA 98195-1700, USA

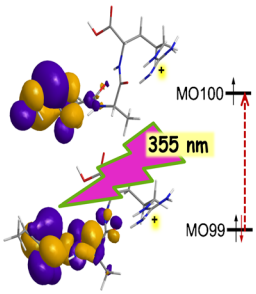

Abstract. Peptide cation-radical fragment ions of the z-type, [$^{\bullet}$AXAR^{+}], [$^{\bullet}$AXAK^{+}], and [$^{\bullet}$XAR^{+}], where X = A, C, D, E, F, G, H, K, L, M, N, P, Y, and W, were generated by electron transfer dissociation of peptide dications and investigated by MS^{3}-near-ultraviolet photodissociation (UVPD) at 355 nm. Laser-pulse dependence measurements indicated that the ion populations were homogeneous for most X residues except phenylalanine. UVPD resulted in dissociations of backbone CO–NH bonds that were accompanied by hydrogen atom transfer, producing fragment ions of the $[y_n]^+$ type. Compared with collision-induced dissociation, UVPD yielded less side-chain dissociations even for residues that are sensitive to radical-induced side-chain bond cleavages. The backbone dissociations are triggered by transitions to second (*B*) excited electronic states in the peptide ion R-CH$^{\bullet}$-CONH- chromophores that are resonant with the 355-nm photon energy. Electron promotion increases the polarity of the *B* excited states, R-CH^{+}-C$^{\bullet}$(O^{-})NH-, and steers the reaction to proceed by transfer of protons from proximate acidic C_{α} and amide nitrogen positions.

Keywords: Electron transfer dissociation, Tryptic peptides, Cation-radical fragments ions, Photodissociation, Excited states

Received: 23 November 2016/Revised: 20 December 2016/Accepted: 21 December 2016/Published Online: 2 February 2017

Introduction

Photodissociation is one of the tools for accomplishing dissociations of gas-phase ions [1–4] that more recently has been widely applied to biomolecular ions [5–13]. Photodissociation in the far UV (157 nm [14, 15]) and middle UV (193 nm [16]) regions of the spectrum has been used to dissociate peptide ions. Recently, photodissociation has been combined with another ion activation method, electron transfer dissociation (ETD) [17], to drive nonselective dissociations of primary peptide fragment ions produced by ETD, thus increasing the number of fragment ions to be potentially used in peptide sequencing [18]. Near-UV photodissociation at 355 nm of ETD peptide fragment ions of the z-type has been shown to be a selective tool for determining the ion structure by targeting the radical chromophores generated by electron transfer [19]. Infrared multiphoton dissociation of ETD-produced peptide fragment ions has also been implemented to provide useful information of the structure and conformation of c- [20] and z-type [21] ions. Whereas UV photo-excitation (UVPD) at 193 nm results in nonspecific dissociation of many bonds in ETD fragment ions, UVPD at 355 nm has been shown to trigger backbone and side-chain bond cleavage that were specific for amino acid residues in the peptide ion [22–26]. When combined with action spectroscopy [9], UV-VIS photodissociation provides information on mass-resolved photodissociation channels pertinent to different excited electronic states of the ion [27, 28].

UVPD differs from the more traditional collision-induced dissociation (CID) in a few important aspects. UV photon absorption is a vertical process that generates a resonant excited electronic state and thus delivers a well-defined excitation energy. In contrast, low-energy CID as employed in ion traps operates in the slow-heating regime of multiple collisions occurring on a millisecond time scale [29] and resulting in vibrational excitation of the ion ground electronic state. The

Electronic supplementary material The online version of this article (doi:10.1007/s13361-016-1586-7) contains supplementary material, which is available to authorized users.

Correspondence to: František Tureček; *e-mail:* turecek@chem.washington.edu

electronic excited state generated by UV photon absorption can decay by a vibronic transition to a highly vibrationally excited ground electronic state to trigger dissociations that are of similar nature as those produced by CID. Since the laser pulses used in UVPD are typically a few nanoseconds wide, vibronic decay after the absorption of the first photon can be followed by absorption of more photons from the same laser pulse that compete with dissociation. Alternatively, dissociation can proceed on the potential energy surface of the pertinent excited electronic state. To distinguish these processes, it is of interest to compare UVPD and CID of a series of peptide ions and point out dissociations that are orthogonal to these ion activation modes. A recent study of tyrosine-containing peptide cation-radicals indeed reported essential differences in dissociations triggered by UV absorption and collisional activation [26].

Here, we report a comparative UVPD study of a series of peptide fragment ions of the z-type. These ions are generated by ETD of a tryptic peptide library AAXAB, where X is a natural amino acid residue (X = A, C, D, E, F, G, H, K, L, M, N, P, R, W) and B is Arg (R) or Lys (K). CID of a related series of AAXAR ions have been analyzed previously [30, 31] and are used here as a reference for matching X residues. We selected to study UVPD of the following types of z-ions. The first type is $[^{\bullet}AXAB^{+}]$, or $[z_4 + H]^{+\bullet}$, ions (for nomenclature see Ref [32]), that have the C_{α}-radical defect at the deaminated *N*-terminal Ala residue and contain a common chromophore for all combinations of X and B. Second, ETD fragment ions by loss of ammonia from peptides of the Lys-C-terminated (AAXAK) series were studied. These correspond to $[^{\bullet}AAXAK^{+}]$, or $[z_5 + H]^{+\bullet}$, ions according to previous studies of ion structure that established that the ammonia molecule selectively originates from the peptide *N*-terminus [33, 34]. Analogous fragment ions by ETD loss of ammonia from the Arg-C-terminated (AAXAR) series were not considered because they are likely to be mixtures of isomers formed by ammonia elimination from the *N*-terminus and the Arg side chain [19, 34]. Third, $[^{\bullet}XAR^{+}]$, or $[z_3 + H]^{+\bullet}$ ions that have the C_{α}-radical defect at the variable X residue were studied for the Arg C-terminated peptides. Photo-induced and collision-induced dissociation pathways of these ion series are analyzed and related to the nature of the X and B residues as well as the excitation mode.

Experimental

Materials and Methods

Synthetic peptides were purchased from NEOPeptide Laboratories (Cambridge, MA, USA) or CHI Scientific (Maynard, MA, USA), and their identity and purity were checked by mass spectrometry. Mass spectra were measured on an LTQ-XL-ETD linear ion trap (LIT) tandem mass spectrometer (ThermoElectron Fisher, San Jose, CA, USA) that has been modified to allow photodissociation studies [19]. Doubly charged peptide ions were generated by electrospray of solutions in 50:50:0.5 methanol-water-acetic acid and mass-selected in the LIT. The $[z_n + H]^{+\bullet}$ fragment ions of interest were formed by electron transfer dissociation using fluoranthene anion radicals as reagent. The $[z_n + H]^{+\bullet}$ ions were mass-selected and exposed to a series of typically 1–10 laser pulses to generate ETD-UVPD-MS^3 spectra. The laser beam at 355 nm was produced from an EKSPLA NL 301 HT Nd–YAG laser (Altos Photonics, Bozeman, MT, USA) providing the third harmonics line at 355 nm, as described previously [19]. The photodissociation yields were measured as a function of the laser power for the $[z_4 + H]^{+\bullet}$ (*m/z* 487) ion from AAWAR and showed approximately linear increase in the range of 3.3–9 mJ/pulse, indicating single photon absorption (Supplementary Figure S1). The computational methods used are described in the Supplement.

Note on Nomenclature

Hydrogen transfers accompanying dissociations of of peptide cation radicals produce fragment ions that differ in the number hydrogen atoms. This feature and the ion charge and electron parity are conveniently expressed by the all-inclusive nomenclature described recently that uses the hydrogen count in neutral peptide fragments as reference [32]. The conversion

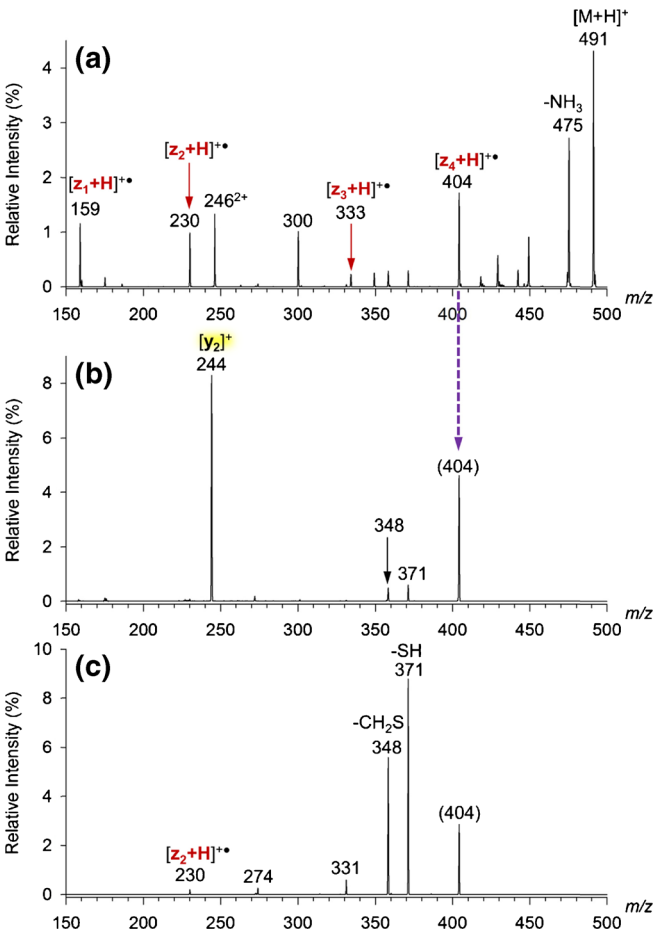

Figure 1. (a) ETD-MS^2 mass spectrum (fluoranthene, 200 ms ion–ion reaction time) of $(AACAK + 2H)^{2+}$ (*m/z* 246); (b) UVPD-MS^3 mass spectrum (single pulse at 355 nm) of the $[z_4 + H]^{+\bullet}$ *m/z* 404 ion from ETD. (c) CID-MS^3 mass spectrum of the $[z_4 + H]^{+\bullet}$ *m/z* 404 ion from ETD

Table 1. Intensities and Assignments from UVPD of $[z_4 + H]^{+\bullet}$ Fragment Ions from AAXAR

	Backbone Cleavages			Side-Chain Dissociations		
Residue (ion *m/z*)	*m/z*	Assignment[a]	Rel. intensity (%)[b, c]	*m/z*	Assignment	Rel. intensity (%)
A (372)	315	$[y_3]^+$	47	*354*	$-H_2O$	*<1*
	244	$[y_2]^+$	9	*328*	$-CO_2$	*<1*
	271	$[x_2]^{+\bullet}$	-	*327*	$-CO_2H$	*<1*
	230	$[z_2 + H]^{+\bullet}$	*5*	298	$-C_2H_8N_3$	3
	175	$[y_1 + 2H]^+$	25			
	159	$[z_1 + H]^{+\bullet}$	11			
C (404)	272	$[x_2 + H]^{+\bullet}$	2	*371*	-SH	*6*
	244	$[y_2]^+$	**87**	*358*	$-SCH_2$	*5*
D (416)	272	$[x_2 + H]^{+\bullet}$	5	372	$-CO_2$	26
	246	$[y_2 + 2H]^+$	2	*371*	-COOH	*7*
	244	$[y_2]^+$	**13**	**315**	$-C_4H_{11}N_3$	**11**
	230	$[z_2 + H]^{+\bullet}$	35			
E (430)	**373**	$[y_3]^+$	**10**	429	-H	9
	358	$[z_3 + H]^{+\bullet}$	12	371	$-C_2H_3O_2$	57
	244	$[y_2]^+$	**8**	301	$-(C_2H_3O_2 + C_3H_5NO)$	2
	230	$[z_2 + H]^{+\bullet}$	4			
F (448)	**391**	$[y_3]^+$	**16**	*404*	$-CO_2$	*<1*
	272	$[x_2 + H]^{+\bullet}$	4			
	244	$[y_2]^+$	**64**			
	230	$[z_2 + H]^{+\bullet}$	16			
G (358)	**301**	$[y_3]^+$	**65**	*340*	$-H_2O$	*<1*
	246	$[y_2 + 2H]^+$	7	*314*	$-CO_2$	*6*
	244	$[y_2]^+$	**20**			
	230	$[z_2 + H]^{+\bullet}$	**2**			
H (438)	**381**	$[y_3]^+$	**22**	**301**	$[z_3 + H]^{+\bullet} - C_3H_3N_2$	**4**
	366	$[z_3 + H]^{+\bullet}$	2			
	272	$[x_2 + H]^{+\bullet}$	12			
	244	$[y_2]^+$	**15**			
	230	$[z_2 + H]^{+\bullet}$	44			
K (429)	**372**	$[y_3]^+$	**21**	413	$-NH_2$	4
	358	$[z_3 + H]^{+\bullet}$	15	*411*	$-H_2O$	*<1*
	272	$[x_2 + H]^{+\bullet}$	2	386	$-C_2H_5N$	5
	244	$[y_2]^+$	**6**	**355**	$-C_2H_8N_3$	**30**
	230	$[z_2 + H]^{+\bullet}$	4	**301**	$[z_3 + H]^{+\bullet} - C_3H_7N$	**4**
				286	$[z_3 + H]^{+\bullet} - C_4H_{10}N$	**9**
L (414)	**357**	$[y_3]^+$	6	371	$-C_3H_7$	38
	244	$[y_2]^+$	**14**	358	$-C_4H_8$	35
	230	$[z_2 + H]^{+\bullet}$	5	**301**	$[z_3 + H]^{+\bullet} - C_3H_6$	**2**
M (432)	**375**	$[y_3]^+$	25	417	$-CH_3$	0.7
	244	$[y_2]^+$	**3**	385	$-SCH_3$	10
	175	$[y_1 + 2H]^+$	3	371	$-CH_2SCH_3$	51
				358	$-C_3H_6S$	7
N (415)	**358**	$[y_3]^+$	**14**	371	$-CONH_2$	43
	272	$[x_2 + H]^{+\bullet}$	6	315	$-C_4H_{10}N_3$	2
	244	$[y_2]^+$	**9**			
	230	$[z_2 + H]^{+\bullet}$	26			
P (398)	341	$[y_3]^+$	71	*354*	$-CO_2$	*<1*
	272	$[x_2]^+$	1	**300**	$-C_5H_8NO$	**10**
	244	$[y_2]^+$	19			
R (457)	**400**	$[y_3]^+$	**19**	439	$-H_2O$	<1
	244	$[y_2]^+$	2	413	$-CO_2$	<1
	230	$[z_2 + H]^{+\bullet}$	8	**385**	$-C_2H_6N_3$	**13**
				383	$-C_2H_8N_3$	**8**
				371	$-C_3H_8N_3$	42
				358	$-C_4H_9N_3$	8

Table 1 (continued)

Residue (ion *m/z*)	Backbone Cleavages			Side-Chain Dissociations		
	m/z	Assignment[a]	Rel. intensity (%)[b, c]	*m/z*	Assignment	Rel. intensity (%)
W (487)	430	$[y_3]^+$	11	443	$-CO_2$	<1
	272	$[x_2 + H]^{+\bullet}$	6	415	$-C_2H_6N_3$	4
	244	$[y_2]^+$	**51**	*358*	$-C_9H_7N$	1
	230	$[z_2 + H]^{+\bullet}$	1	**301**	$[z_3 + H]^{+\bullet} - C_8H_5N$	**2**
	175	$[y_1 + 2H]^+$	4			
	159	$[z_1 + H]^{+\bullet}$	4			

[a]The all-inclusive fragment ion nomenclature is used [32]. Conversion to the Roepstorff-Fohlman-Biemann system [35, 36] is as follows: $[y_n]^+ = (\boldsymbol{y_n} - 2H)^+$; $[y_n + 2H]^+ = \boldsymbol{y_n}$; $[z_n + H]^{+\bullet} = \boldsymbol{z_n}$; $[x_n + H]^{+\bullet} = \boldsymbol{x_n}$.
[b]CID fragment ions whose relative intensities exceed ten fold those from UVPD are given as italics.
[c]UVPD fragment ions whose relative intensities exceed ten fold those from CID are given as bold characters.

to the common Roepstorff-Fohlman-Biemann nomenclature [35, 36] is as follows for the fragment ions described here: $[z_n + H]^{+\bullet} = z_n$, $[z_n]^+ = z_n - 1 = w_n$, $[x_m + H]^{+\bullet} = x_m$, $[y_i + 2H]^+ = y_i$, $[y_i]^+ = y_i - 2 = v_n$.

Results

The ions of interest were generated by ETD of doubly charged peptide ions, as illustrated with AACAR (*m/z* 246, Figure 1a). The ETD-produced $[z_4 + H]^{+\bullet}$ and $[z_3 + H]^{+\bullet}$ ions at *m/z* 404 and 333, respectively, were selected by mass and exposed to laser pulses at 355 nm. Note that the $[z_3 + H]^{+\bullet}$ ion from ETD undergoes spontaneous loss of SH radical to *m/z* 300 that decreases the primary fragment ion intensity [34, 37]. The single-pulse UVPD-MS^3 spectrum of the $[z_4 + H]^{+\bullet}$ ion (Figure 1b) shows a dominant backbone dissociation of the Cys–Ala amide bond, forming the $[y_2]^+$ fragment ion at *m/z* 244. This dissociation requires a hydrogen atom migration to the departing neutral fragment, as studied previously [19, 23]. In contrast, CID of the $[z_4 + H]^{+\bullet}$ ion results in dominant Cys side-chain dissociations [30, 31] while backbone cleavages are competitively suppressed. The UVPD and CID spectra of all the $[z_4 + H]^{+\bullet}$ ions from AAXAR are summarized in Table 1. The UVPD relative intensities were normalized to the sum of the fragment ions in the MS^3 spectra. To highlight the differences in the UVPD and CID spectra, we denote as *significantly specific* the MS^3 fragment ions that show a 10-fold difference in relative intensity in either spectrum. The fragment ions that are more than 10-fold abundant upon UVPD are shown in bold characters, those more than 10-fold abundant upon CID are given as italics in Table 1. Fragment ions appearing in both types of spectra, albeit at different relative intensities, are shown as regular characters. The Table 1 data indicate three types of photodissociation reactions of the Arg-C-terminated $[z_4 + H]^{+\bullet}$ ions : (1) amide CO–NH bond cleavages leading to $[y_n]^+$ ions, (2) N–C_α bond cleavages leading to $[z_2 + H]^{+\bullet}$ ions [30, 31], and (3) residue-specific side-chain dissociations. Peptide ions with residues lacking reactive side chains (G, A, P) gave dominant $[y_3]^+$ photofragment ions, resulting from cleavage of the CO–NH bond next to the *N*-terminal radical carrying residue and involving a hydrogen transfer onto the departing C_3H_5O radical (Scheme 1).

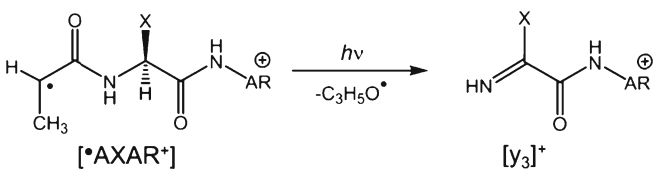

Scheme 1. Formation of $[y_3]^+$ fragment ions

Residues that are potentially susceptible to radical-induced side-chain dissociations [37–39] showed mixed results. With $[z_4 + H]^{+\bullet}$ ions containing Asp, Asn, Glu, Leu, Arg, and Met, side-chain dissociations were abundant, although they did not outcompete backbone CO–NH cleavages forming the $[y_3]^+$ and $[y_2]^+$ ions. Remarkably, the photodissociative SH loss from the Cys side-chain was only minor (Figure 1b), whereas it was predominant in the CID spectrum. Likewise, the internal Lys residue did not undergo extensive radical side-chain dissociations [37], the main side-chain loss of $C_2H_8N_3$ occurring from the C-terminal Arg residue. An interesting comparison can be made for $[z_4 + H]^{+\bullet}$ ions containing residues that are known to favor cascade N–C_α bond cleavages leading to $[z_2 + H]^{+\bullet}$ ions (Asp, Asn, Phe, His, and Trp) [30, 31]. Among these, Asp, Asn, and His gave abundant $[z_2 + H]^{+\bullet}$ photofragments that competed with the formation of the $[y_n]^+$ ions. In contrast, Phe and Trp produced dominant $[y_2]^+$ photofragments that were virtually absent in the CID spectra.

The photodissociations of the Lys-C-terminated $[z_4 + H]^{+\bullet}$ ions are compiled in Table 2.

The backbone CO–NH bond and side-chain dissociations follow a similar trend as observed for the analogous Arg-C-terminated ions. The combined relative intensities of the $[y_3]^+$ and $[y_2]^+$ UVPD fragment ions from $[^\bullet AXAR^+]$ and $[^\bullet AXAK^+]$ are summarized in Figure 2. A novel feature with the $[^\bullet AXAK^+]$ series is the more pronounced photodissociative loss of water from Ala-, Phe-, and His-containing ions that was not observed for the Arg-C-terminated ions. Another distinctive feature is the enhanced elimination of ammonia from the $[y_3]^+$ ions from the His- and Arg-containing ions. It should be noted that the diagnostic $[z_2 + H]^{+\bullet}$ ions in this series (*m/z* 202) overlap with a background peak of photo-ionized fluoranthene and thus their relative intensities could not be quantified.

Table 2. Intensities and Assignments from UVPD of $[z_4 + H]^{+\bullet}$ Fragment Ions from AAXAK

	Backbone Cleavages			Side-Chain Dissociations		
Residue (ion m/z)	*m/z*	Assignment[a]	Rel. intensity (%)[b, c]	*m/z*	Assignment	Rel. intensity (%)
A (344)	287	$[y_3]^+$	33	326	$-H_2O$	30
	217	$[y_2 + H]^{+\bullet}$		*285*	$-C_3H_9N$	
	216	$[y_2]^+$	**36**	*273*	$-C_4H_{11}N$	
D (388)	**287**	$[y_3]^+ - CO_2$	**6**	*370*	$-H_2O$	
	270	$287 - NH_3$	**4**	344	$-CO_2$	45
	245	$[x_2 + H]^{+\bullet}$	8	326	$-(CO_2 + H_2O)$	6
	218	$[y_2 + 2H]^+$	14			
	217	$[y_2 + H]^{+\bullet}$				
	216	$[y_2]^+$	17			
E (402)	345	$[y_3]^+$	6	*384*	$-H_2O$	*<1*
	330	$[z_3]^+$	21	343	$-C_2H_3O_2$	61
	218	$[y_2 + 2H]^+$	5			
	217	$[y_2 + H]^{+\bullet}$				
	216	$[y_2]^+$	**7**			
F (420)	363	$[y_3]^+$	35	402	$-H_2O$	12
	349	$[z_3 + H]^{+\bullet}$	4			
	346		7			
	293		5			
	245	$[x_2 + H]^{+\bullet}$	12			
	216	$[y_2]^+$	22			
	202[d]	$[z_2 + H]^{+\bullet}$				
G (330)	216	$[y_2]^+$		312	$-H_2O$	
				279		
H (410)	353	$[y_3]^+$	19	392	$-H_2O$	23
	336	$[y_3]^+ - NH_3$	**24**	352	$-C_3H_8N$	9
	218	$[y_2 + 2H]^+$	14			
	216	$[y_2]^+$	11			
	202[d]	$[z_2 + H]^{+\bullet}$				
L (386)	218	$[y_2 + 2H]^+$	10	*368*	$-H_2O$	
	216	$[y_2]^+$	6	343	$-C_3H_7$	34
	202[d]	$[z_2 + H]^{+\bullet}$		330	$-C_4H_8$	42
				270		8
N (387)	330	$[y_3]^+$	17	369	$-H_2O$	5
	245	$[x_2 + H]^{+\bullet}$	6	343	$-CONH_2$	33
	218	$[y_2 + 2H]^+$	15	270		7
	216	$[y_2]^+$	17			
	202[d]	$[z_2 + H]^{+\bullet}$				
R (429)	**372**	$[y_3]^+$	**19**	**428**	-H	**29**
	355	$[y_3]^+ - NH_3$	**6**	*411*	$-H_2O$	<1
	218	$[y_2 + 2H]^+$	20	*385*	$-CO_2$	<1
	216	$[y_2]^+$	24	*342*	$-C_3H_9N_3$	<1
				371	$-CH_4N_3$	9
S (360)	218	$[y_2 + 2H]^+$	6	342	$-H_2O$	37
				330	$-CH_2O$	6
				287	$-C_4H_{11}N$	51
T (374)	218	$[y_2 + 2H]^+$	8	356	$-H_2O$	51
	216	$[y_2]^+$	5	330	$-C_2H_4O$	7
				302	$-C_4H_{11}N$	8
				301	$-C_4H_{11}N$	16
				256	301 - COOH	5
Y (436)	**379**	$[y_3]^+$	**22**	418	$-H_2O$	8
	245	$[x_2 + H]^{+\bullet}$		330	$-C_7H_6O$	4
	218	$[y_2 + 2H]^+$	30			
	216	$[y_2]^+$	35			
	202[d]	$[z_2 + H]^{+\bullet}$				

[a]The all-inclusive fragment ion nomenclature is used [32]. Conversion to the Roepstorff-Fohlman-Biemann system [35, 36] is as follows: $[y_n]^+ = (\boldsymbol{y_n} - 2H)^+$; $[y_n + 2H]^+ = \boldsymbol{y_n}$; $[z_n + H]^{+\bullet} = \boldsymbol{z_n}$; $[x_n + H]^{+\bullet} = \boldsymbol{x_n}$.

[b]CID fragment ions whose relative intensities exceed ten fold those from UVPD are given as italics.

[c]UVPD fragment ions whose relative intensities exceed ten fold those from CID are given as bold characters.

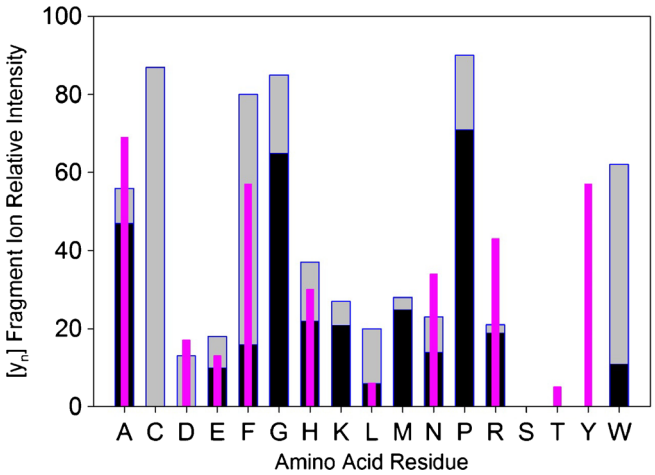

Figure 2. UVPD relative intensities of $[y_3]^+$ and $[y_2]^+$ fragment ions. Black bars: $[y_3]^+$ relative intensities from $[^{\bullet}AXAR^+]$; gray bars: $[y_2]^+$ relative intensities from $[^{\bullet}AXAR^+]$; magenta bars: combined $[y_3]^+$ and $[y_2]^+$ relative intensities from $[^{\bullet}AXAK^+]$

Moving the radical site one Ala residue away, as in $[z_5 + H]^{+\bullet}$ Lys-C-terminated ions, resulted in homologous shifts and enhancement of the $[y_n]^+$ photofragment ions. For most $[z_5 + H]^{+\bullet}$, UVPD produced diagnostic $[y_4]^+$, $[y_3]^+$, and $[y_2]^+$ fragment ions, enhancing sequence readout. Conversely, radical-induced side-chain eliminations, such as loss of CO_2 from Asp, $CONH_2$ from Asn, $C_2H_3O_2$ from Glu, C_4H_8 from Leu, and H_2O from Ser and Thr, were less prominent than for the $[z_4 + H]^{+\bullet}$ ions. Another common feature was that the $[y_n]^+$ ions underwent further loss of ammonia (Table 3). A distinctively different UVPD spectrum was produced from the Arg-containing $[z_5 + H]^{+\bullet}$ ion, $[^{\bullet}AARAK^+]$, which showed the formation of $[z_3]^+$ ions (w_3 according to the Biemann nomenclature) and their secondary dissociation products by loss of ammonia (Table 3). These differences are probably related to the mechanism of NH_3 loss from $[AARAK + 2H]^{+\bullet}$ that can involve the *N*-terminus as well as the Arg side chain, producing isomeric ions. Nevertheless, the UVPD and CID spectra of this ion were quite distinct, indicating different dissociations proceeding from the ground and excited electronic state.

Pulse Dependence

Further information about the nature of the ETD fragment ions can be obtained from pulse-dependent UVPD measurements [25]. The first pulse induces dissociation of light-absorbing ions at the selected wavelength. The product ions that are closed-shell species, such as the $[y_n]^+$ ions, do not absorb light at 355 nm and are inactive upon irradiation with subsequent laser pulses. The relative intensities of these ions increase with the number of laser pulses. Cation-radical product ions, for example the $[z_2 + H]^{+\bullet}$ ions, absorb light at 355 nm and are photolyzed upon subsequent exposure to laser pulses. The relative intensities of these ions grow to a maximum and then decrease. This is illustrated with pulse-dependent UVPD relative ion intensities of the $[z_2 + H]^{+\bullet}$ and $[y_3]^+$ fragment ions from $[^{\bullet}AHAR^+]$ (Figure 3). Fitting the $[^{\bullet}AHAR^+]$ ion relative intensity with a single exponential function, $I(n) = I_0e^{-0.3669n}$, where I_0 is the initial normalized ion intensity and $I(n)$ is the normalized intensity after n laser pulses, gives the broken-line curve in Figure 3 with a root-mean square deviation, RMSD = 2.7%. However, a substantially tighter fit (RMSD = 1.2%) can be obtained by fitting in a two-parameter formula,

$I(n) = I_0(0.94e^{-0.3669n} + 0.06)$, which includes a 6% fraction of non-photodegradable residual ions, as shown by the solid blue line curve in Figure 3.

In general terms, ion photodepletion upon laser irradiation can follow an exponential decay law (Equation 1), where I_0 is the initial molar fraction of the photo-active species, $I(n)$ is the normalized intensity after n laser pulses, and $\alpha > 0$ is the photodissociation efficiency per pulse,

$$I(n) = I_0e^{-n\alpha} \quad (1)$$

that depends on the photon flux (Φ) and the wavelength-dependent ion absorption cross-section (σ), $\alpha = \Phi\sigma$. Equation 1 applies when the ion population is homogeneous and every photon absorption is dissociative on the time scale of the experiment, which is often justified by the low activation energies for radical dissociations [23, 25, 31, 40, 41] and the substantial excitation energy delivered by the photon (3.49 eV or 337 kJ mol^{-1} at 355 nm). Table 4 data indicate that $[z_4 + H]^{+\bullet}$ ions from most peptide sequences follow a single exponential decay law. However, if the ion population initially contains a molar fraction $x_0(M_2)$ of an isomer M_2 that does not absorb at 355 nm, the photodepletion process follows Equation 2, where $I(n)$ converges to $I_0x_0(M_2)$.

$$\frac{I(n)}{I_0} = x_0(M_1)e^{-n\alpha} + x_0(M_2) \quad (2)$$

An even more general scenario has been considered previously for photodissociation of peptide cation-radicals, whereby the photo-active ions (M_1) of an initial molar fraction equal to $x_0(M_1)$ competitively dissociate with efficiency α and isomerize with efficiency β to a new isomer (M_3), which then photodissociates with efficiency γ (Equation 3) [22]. For $\beta = 0$ (no photo-isomerization), Equation 3 reduces to Equation 2.

$$\frac{I(n)}{I_0} = \frac{x_0(M_1)}{\alpha + \beta - \gamma}\left[(\alpha - \gamma)e^{-(\alpha+\beta)n} + \beta e^{-\gamma n}\right] + x_0(M_2) \quad (3)$$

The data in Table 4 indicate that most peptide ions do not contain photostable isomers either initially present or produced by photo-isomerization. Analysis of Equation 3 for several combinations of the α, β, and γ parameters indicates that increasing β and decreasing γ relative to α results in a slower photodepletion. However, Equation 3 curves where $x_0(M_2) = 0$ can be fitted with single exponential decay functions with RMSD <4% showing an apparent lower photodissociation

Table 3. Intensities and Assignments in UVPD of $[z_5 + H]^{+\bullet}$ Fragment Ions from AAXAK

	Backbone Cleavages			Side-Chain Dissociations		
Residue (ion *m/z*)	*m/z*	assignment[a]	rel. intensity (%)[b,c]	*m/z*	assignment	rel. intensity (%)
A (415)	358	$[y_4]^+$	20			
	341	$[z_4 - H]^+$	**4**			
	287	$[y_3]^+$	28			
	270	$[z_3 - H]^+$	16			
	218	$[y_2 + 2H]^+$	**10**			
	216	$[y_2]^+$	**22**			
D (459)	**402**	$[y_4]^+$	**22**	*441*	$-H_2O$	<0.1
	385	$[z_4 - H]^+$	**4**	**431**	-CO	**2**
	314	$[z_3 - H]^+$	6	415	$-CO_2$	15
	270	$287 - NH_3$	5	*400*	$-C_3H_9N$	*<1*
	218	$[y_2 + 2H]^+$	**12**	*388*	$-C_4H_{10}N$	*<1*
	216	$[y_2]^+$	**25**	**287**	$[y_3 - CO_2]^+$	**7**
E (473)	**416**	$[y_4]^+$	**30**	455	$-H_2O$	<1
	401	$[z_4 - H]^+$	*3*	414	$-C_2H_3O_2$	15
	399	$[y_4 - NH_3]^+$	**7**			
	345	$[y_3]^+$	**4**			
	328	$[y_3 - NH_3]^+$	4			
	272	$[w_3]^+$	4			
	257		9			
	218	$[y_2 + 2H]^+$	10			
	217	$[y_2 + H]^{+\bullet}$				
	216	$[y_2]^+$	**17**			
F (491)	434	$[y_4]^+$	18	*473*	$-H_2O$	
	417		4	**463**	-CO	**3**
	363	$[y_3]^+$	31	*432*	$-C_3H_9N$	
	346	$[y_3 - NH_3]^+$	7	*420*	$-C_4H_9N$	
	275		10			
	218	$[y_2 + 2H]^+$	10			
	216	$[y_2]^+$	15			
H (481)	424	$[y_4]^+$	18	*463*	$-H_2O$	
	407	$[y_4 - NH_3]^+$	**12**	423	$-C_3H_8N$	7
	353	$[y_3]^+$	6	410	$-C_4H_{11}N$	4
	336	$[y_3 - NH_3]^+$	**24**			
	318		2			
	309		5			
	264		2			
	246					
	238		7			
	237		13			
	202[d]					
L (457)	**400**	$[y_4]^+$	**34**	*439*	$-H_2O$	<1
	383	$[y_4 - NH_3]^+$	**6**	414	$-C_3H_7$	9
	339		2	401	$-C_4H_8$	20
	329	$[y_3]^+$	**8**	386	$-C_4H_9N$	<1
	312	$[y_3 - NH_3]^+$	5			
	272		4			
	218	$[y_2 + 2H]^+$	**4**			
	216	$[y_2]^+$	**9**			
N (458)	**401**	$[y_4]^+$	**17**	*440*	$-H_2O$	*1*
	387	$[y_4 - NH_3]^+$	**3**	**430**	-CO	**4**
	384		4	414	$-CONH_2$	13
	330	$[y_3]^+$	**24**			
	313	$[y_3 - NH_3]^+$	6			
	287		5			
	270		4			
	218	$[y_2 + 2H]^+$	**5**			
	216	$[y_2]^+$	**8**			
	202[d]	$[z_2 + H]^{+\bullet}$				
R (500)	372	$[y_3]^+$	1	**499**	-H	**25**
	357	$[z_3]^+$	**25**	*482*	$-H_2O$	*<1*

Table 3 (continued)

Residue (ion *m/z*)	Backbone Cleavages			Side-Chain Dissociations		
	m/z	assignment[a]	rel. intensity (%)[b,c]	*m/z*	assignment	rel. intensity (%)
	340	$[z_3 - NH_3]^+$	**16**	*456*		*<1*
	323	$[z_3 - 2NH_3]^+$	**4**	429	$-C_4H_9N$	17
	313		**7**	413	$-C_3H_9N_3$	<1
	270		1			
	256		2			
S (431)	**374**	$[y_4]^+$	**35**	*413*	$-H_2$	*3*
	357	$[y_4 - NH_3]^+$	**14**	*401*	$-CH_2O$	
	339	$[357 - H_2O]^+$	2	*360*	$-C_4H_{11}N$	
	313		4			
	303	$[y_3]^+$	**4**			
	288	$[z_3]^+$	<1			
	287	$[z_3 - H]^{+\bullet}$	3			
	268		6			
	218	$[y_2 + 2H]^+$	7			
	216	$[y_2]^+$	**21**			
T (445)	388	$[y_4]^+$	34	*427*	$-H_2O$	*3*
	371	$[y_4 - NH_3]^+$	13	*401*	$-C_2H_4O$	
	353	$[371 - H_2O]^+$	2	374	$-C_4H_{11}N$	2
	327		6			
	302	$[z_3]^+$	2			
	301	$[z_3 - H]^{+\bullet}$	2			
	229		10			
	218	$[y_2 + 2H]^+$	5			
	216	$[y_2]^+$	14			
Y (507)	450	$[y_4]^+$	19	*489*	$-H_2O$	
	433	$[y_4 - NH_3]^+$	4	479	$-CO$	3
	379	$[y_3]^+$	**26**	*436*	$-C_4H_{11}N$	
	362	$[y_3 - NH_3]^+$	8	401	$-C_7H_6O$	19
	336		3			
	291		10			
	218	$[y_2 + 2H]^+$	7			
	216	$[y_2]^+$	17			
	202[d]	$[z_2 + H]^{+\bullet}$				

[a]The all-inclusive fragment ion nomenclature is used [32]. Conversion to the Roepstorff-Fohlman-Biemann system [35, 36] is as follows: $[y_n]^+ = (\boldsymbol{y_n} - 2H)^+$; $[y_n + 2H]^+ = \boldsymbol{y_n}$; $[z_n + H]^{+\bullet} = \boldsymbol{z_n}$; $[x_n + H]^{+\bullet} = \boldsymbol{x_n}$.
[b]CID fragment ions whose relative intensities exceed ten fold those from UVPD are given as italics.
[c]UVPD fragment ions whose relative intensities exceed ten fold those from CID are given as bold characters.
[d]Overlapped with photodesorbed fluoranthene ions.

efficiency $\alpha_{eff} < \alpha$. Thus, it is difficult to distinguish from the pulse dependence alone whether the ion undergoes only photodissociation or whether the dissociation is accompanied by the formation of another photoactive isomer. Distinction has been made for [•AFAR+] ions using single-pulse action spectroscopy that clearly indicated the presence of two $[z_4 + H]^{+\bullet}$ ion isomers produced by ETD [27]. It should be noted that the data reported in Ref 27 were obtained at a lower laser power (0.8–2.1 mJ/pulse) than the present 355 nm data, which accounts for the different α_{eff}.

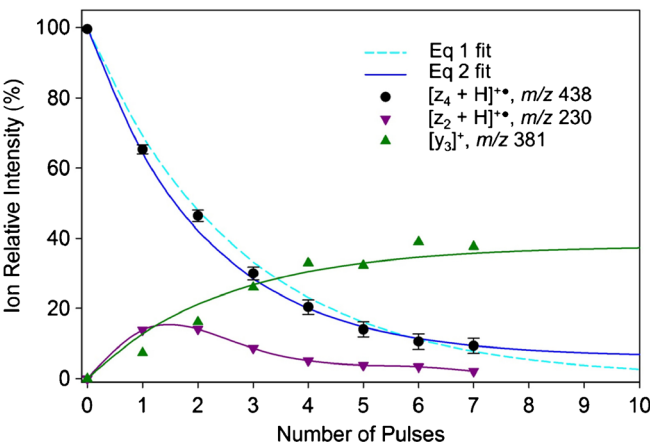

Figure 3. Laser pulse dependence of selected photofragment ion intensities from [•AHAR+] (*m/z* 438)

$[z_4 + H]^{+\bullet}$ Ions

The Table 4 data rank the photodissociation efficiencies of the $[z_4 + H]^{+\bullet}$ ions. The light-absorbing chromophore at 355 nm in all these ions is the Ala C_α radical [25]. The electron transitions leading to the second (*B*) doublet excited state (ΔE_{exc} = 3.509 eV, 353 nm, oscillator strength *f* = 0.024) are shown for [•AAAR+] (Figure 4). These transitions lead to absorption at 355 nm and photodissociation; note, however, that the absorption maximum is

Table 4. Photodissociation Efficiencies of $^{\bullet}AXAR^{+}$ $[z_4 + H]^{+\bullet}$ Ions at 355 nm

Residue X	α_{eff}[a]	$x_0(M_2)$[a]	RMSD (%)
P	0.226	0	0.7
R	0.292	0	4.2
G	0.302	0	10.9
H	0.478	0.06	1.2
K	0.548	0	8.8
C	0.567	0	10.9
N	0.686	0	2.6
D	0.689	0	6.6
E	0.710	0	6.1
A	0.702	0	10.9
F	0.721	0.20	2.5
L	0.742	0	1.8
W	0.895	0	5.9
M	0.978	0	1.2

[a] From least square fits to Equation 2.

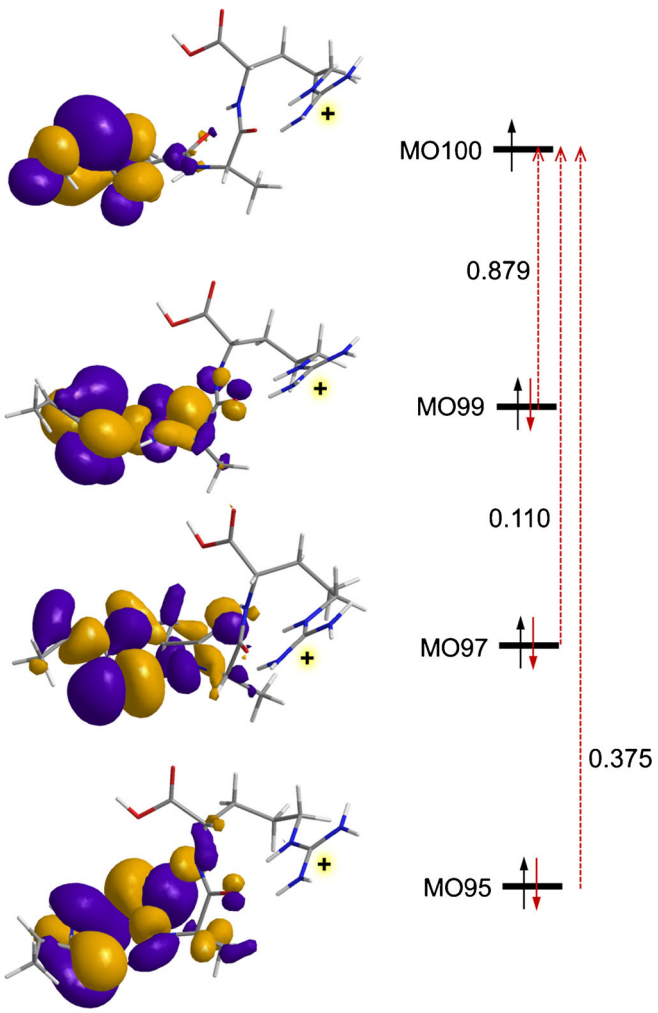

Figure 4. Molecular orbitals involved in electronic excitation to the *B* state of $[^{\bullet}AAAR^{+}]$ (ΔE_{exc} = 3.51 eV, 353 nm, f = 0.024). From ωB97X-D/6-311++G(2d,p) time-dependent DFT calculations. The calculated transition vector amplitudes from the inner beta molecular orbitals (MO95, MO97, and MO99) to the SOMO (MO100) are shown next to the *red arrows*

likely to be red-shifted by vibronic broadening at ambient temperature [42]. The first (*A*) doublet excited state is dark (ΔE_{exc} = 3.19 eV, 388 nm, f = 0.0001). The *B* state excitations involve transitions to the semi-occupied π_z molecular orbital (MO100) starting from the underlying doubly occupied π_z (MO99 and MO95) and π_{xy} (MO97) orbitals. All the involved MOs are delocalized over the *N*-terminal $CH_3CH^{\bullet}CONH$ group with very little involvement of the more remote amide, carboxyl, or guanidine π-electron systems. This suggests that similar types of excitations can be expected for all $[^{\bullet}AXAR^{+}]$ ions with saturated side chains (G, K, L, P) lacking π or lone pair electrons and possibly also for Arg. In spite of this common trait, the $[^{\bullet}AXAR^{+}]$ (X = G, K, L, P, R) ions show different photodissociation efficiencies, $\alpha_{eff}(P) < \alpha_{eff}(R) < \alpha_{eff}(G) < \alpha_{eff}(K) < \alpha_{eff}(A) < \alpha_{eff}(L)$. These large differences cannot be attributed to variations of the laser power, which was calibrated to be within ±10%. Changes in the position of the pertinent ion absorption band would affect the absorbance at 355 nm. These can be caused by different conformations of the $[^{\bullet}AXAR^{+}]$ ions depending on the X residue. However, time-dependent DFT calculations of several ion conformers indicated only minor effects of ion conformation on the 355 nm absorption band position [27]. The high photodissociation efficiency of $[^{\bullet}ALAR^{+}]$ can be associated with the facile dissociation by loss of the Leu side chain (Table 1). With the other residues in this group, photo-induced hydrogen migrations among the C_α positions [23] can deplete the initial *N*-terminal chromophore and affect absorption at 355 nm. Residues possessing π-electron systems (H, N, D, F, W) or lone pairs (C, M) may undergo electron transitions involving these orbitals; a detailed description of these interactions would require a substantial effort in analyzing the pertinent ion conformers and their electronic excitations.

$[z_3 + H]^{+\bullet}$ *Ions*

These cation-radical ETD fragment ions have the radical sites at the C_α position of the variable X residue. This greatly affects

Table 5. Photodissociation at 355 nm of $[z_3 + H]^{+\bullet}$ Ions from AAXAR Peptides

Residue X	α_{eff}[a]	$x_0(M_2)$[a]	RMSD (%)	Major fragment ions
H	0.308	0	6.1	–H, $[y_2]^+$
M	0.343	0	6.4	$–CH_3$, $–C_2H_5S$, $[y_2]^+$
K	0.357	0	0	–H, $–C_3H_6N$, $[y_2]^+$
D	0.374	0.412	5.0	$[y_2]^+$, $[z_2 + H]^{+\bullet}$
N	0.452	0	5.3	$–CH_2CONH_2$, $[y_2]^+$
W	0.463	0.024	13.6	$[y_2]^+$, $[x_2]^+$
G	0.510	0	16.4	$[y_2]^+$
F	0.533	0.394	4.4	$[y_2]^+$, $[x_2]^+$
R	0.614	0	1.3	–H, $–C_3H_8N_3$, $[y_2]^+$
E	0.682	0	2.2	$–C_2H_3O_2$, $[y_2]^+$
A	0.741	0.093	21.7	$[y_2]^+$
L	1.161	0	2.9	$–C_3H_7$

[a] From least square fits to Equation 2.

the ion dissociations, as summarized in Table 5. UVPD of the $[z_3 + H]^{+\bullet}$ ions gives both sequence $[y_2]^+$ fragment ions and products of side-chain cleavages. $[^{\bullet}LAR^+]$ is the only sequence that dissociates entirely by side-chain loss. UVPD of the $[z_3 + H]^{+\bullet}$ with aromatic residues (Phe and Trp) also produces $[x_2]^+$ fragment ions in addition to $[y_2]^+$ ions. The photodissociation efficiencies (α_{eff}) of the $[z_3 + H]^{+\bullet}$ ions follow a different order than those for $[z_4 + H]^{+\bullet}$. Notably, $[^{\bullet}FAR^+]$ and $[^{\bullet}DAR^+]$ show large populations of photostable ion isomers, and mixtures are also indicated for $[^{\bullet}AAR^+]$ and $[^{\bullet}WAR^+]$. In contrast to UVPD, CID of the $[z_3 + H]^{+\bullet}$ mainly results in CO_2 loss or side-chain dissociations, yielding only minor sequence fragment ions (Supplementary Figures S2–S14). The aromatic residues (Phe, Trp) are exceptional in that they produce $[z_2 + H]^{+\bullet}$ sequence fragment ions upon CID, in similarity with CID of higher homologous $[z_n + H]^{+\bullet}$ ions [30, 31].

Discussion

The main feature distinguishing the UVPD and CID spectra of the $[z_n + H]^{+\bullet}$ ions is the facile photodissociative CO–NH bond cleavages forming $[y_{n-1}]^+$ fragment ions. By stoichiometry, this dissociation must involve a hydrogen atom migration onto the neutral fragments, and this raises the question of why the CO–NH bond cleavage is promoted relative to the other

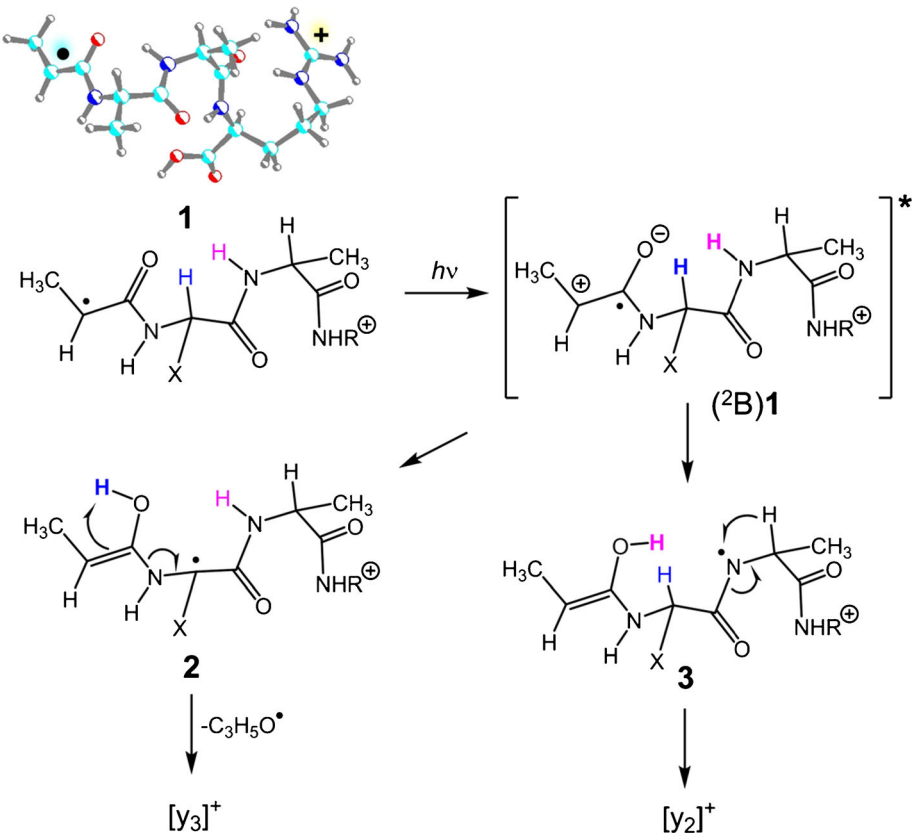

Scheme 2. Proposed mechanism for the formation of $[y_3]^+$ and $[y_2]^+$ fragment ions

dissociations that also involve hydrogen migrations. UVPD and CID differ in the mode of ion excitation. Absorption of a UV photon leads to a sudden formation of an excited electronic state of the ion, and the deposited energy can be used to drive dissociation or dissipated by collisions with the bath gas. Hence, one may posit that photodissociation should be fast and thus reactions with loose transition states should be preferred. However, previous analysis of potential energy surfaces for $[z_4 + H]^{+\bullet}$ ions from AASAR [23], AAAAR [25], AAHAR, AAWAR [31], AAHAL [41], and several other peptide cation-radicals [43–53] suggested that the backbone and side-chain dissociations were of similar type, involving radical-induced hydrogen atom migrations through five- and six-membered transition states of very similar energies [23, 31, 41]. Hence, energy arguments alone are insufficient to explain the preferred formation of $[y_3]^+$ and $[y_2]^+$ fragment ions in UVPD. We now argue that these dissociations proceed from the *B* excited electronic state generated by 355-nm photon absorption. A prerequisite step in the hydrogen migrations occurring in the ground electronic state is amide trans → cis rotation that is necessary to allow the C_α radical to approach the hydrogen atoms to be transferred. This step can be avoided in the excited electronic state. Electronic excitation results in electron density flow from C_α to the adjacent C=O group (Scheme 2). The excitation increases the basicity of the amide oxygen that can abstract the labile proton from the C_α position at the adjacent X residue or from the next amide group.

The optimized structure of $[^{\bullet}AAAR^+]$ (1, Scheme 2) [25] indicates a close proximity of the reactive amide oxygen to the C_α and amide protons. The hydrogen transfer can be formulated as proton-coupled electron transfer [54, 55], reconstituting the electron density distribution in the intermediates and creating reactive radical sites at the C_α and amide nitrogen (Scheme 2). This polar mechanism, involving enolimine intermediates, can account for the preferred transfer of acidic hydrogen atoms, steering the reaction to radical-induced CO–NH bond dissociations. Note that this is fundamentally different from the standard "mobile proton" model of peptide ion dissociations [56–58] where the C_α-H and amide N-H are not engaged in dissociations proceeding in the ground electronic state. The calculated energy balance for the Scheme 2 reactions, when based on ωB97X-D/6-311++G(2d,p) and zero-point energies, indicates that a transition from the *B* excited state of $[^{\bullet}AAAR^+]$ to the C_α enol isomer 2 is 264 kJ mol^{-1} exothermic. Furthermore, the excitation energy is sufficient to drive the C(OH)–NH bond dissociation in 2 where it requires 177 kJ mol^{-1} (251 kJ mol^{-1} relative to 1). At the same time, the enolimine mechanism is unlikely to operate in the ground electronic state of the ion because intermediates 2 and 3 are high-energy isomers of the more conventional amides [31]. The ground-state reactions, as observed in CID, then can be formulated by conventional radical chemistry involving C_α and side-chain hydrogen migrations combined with amide trans-cis isomerizations [23, 25, 31, 41].

Conclusions

Cation-radical $[z_n + H]^{+\bullet}$ fragment ions produced by electron transfer dissociation of tryptic peptides undergo efficient and residue-specific photodissociations at 355 nm. The common feature of this near-UV photodissociation is radical-induced backbone CO—NH bond cleavages accompanied by hydrogen transfer and forming $[y_n]^+$ sequence fragment ions. The photodissociation is associated with C_α radical amide chromophores that undergo electron transitions to second (*B*) excited states to drive proton transfer and backbone cleavages.

Acknowledgments

This research has received funding from the National Science Foundation Division of Chemistry (grant CHE-1359810). F.T. thanks the Klaus and Mary Ann Saegebarth Endowment for support. The authors thank Dr. Christopher J. Shaffer for technical assistance with laser photodissociation measurements.

References

1. Dunbar, R.C.: Photodissociation of the methyl chloride (CH_3Cl^+) and nitrous oxide (N_2O^+) cations. J. Am. Chem. Soc. **93**, 4354–4358 (1971)
2. Casassa, M.P., Bomse, D.S., Beauchamp, J.L., Janda, K.C.: Infrared photochemistry of ethylene clusters. J. Chem. Phys. **72**, 6805–6806 (1980)
3. Carlin, T.J., Freiser, B.S.: Multiphoton ionization in Fourier transform mass spectrometry. Anal. Chem. **55**, 955–958 (1983)
4. Bensimon, M., Rapin, J., Gaumann, T.: Comparison of infrared photodissociation in a Fourier transform mass spectrometer with metastable ion decay in a double-focusing mass spectrometer. Int. J. Mass Spectrom. Ion Process. **72**, 125–135 (1986)
5. Eyler. J.R.: Infrared multiple photon dissociation spectroscopy of ions in Penning traps. Mass Spectrom. Rev. 28, 448–467 (2009)
6. Polfer, N.C.: Infrared multiple photon dissociation spectroscopy of trapped ions. Chem. Soc. Rev. **40**, 2211–2221 (2011)
7. Brodbelt, J.S., Wilson, J.J.: Infrared multiphoton dissociation in quadrupole ion traps. Mass Spectrom. Rev. **28**, 390–424 (2009)
8. Dunbar, R.C.: Spectroscopy of metal-ion complexes with peptide-related ligands. Top. Curr. Chem. **364**, 183–223 (2015)
9. Antoine, R., Dugourd, P.: Visible and ultraviolet spectroscopy of gas phase protein ions. Phys. Chem. Chem. Phys. **13**, 16494–16509 (2011)
10. Antoine, R., Dugourd, P.: UV-visible activation of biomolecular ions. Lect. Notes Chem. **83**, 93–116 (2013)
11. Byskov, C.S., Jensen, F., Jorgensen, T.J.D., Nielsen, S.B.: On the photostability of peptides after selective photo-excitation of the backbone: prompt versus slow dissociation. Phys. Chem. Chem. Phys. **16**, 15831–15838 (2014)
12. Hendricks, N.G., Lareau, N.M., Stow, S.M., McLean, J.A., Julian, R.R.: Bond-specific dissociation following excitation energy transfer for distance constraint determination in the gas phase. J. Am. Chem. Soc. **136**, 13363–13370 (2014)
13. Lai, C.-K., Ng, D.C.M., Pang, H.F., Le Blanc, J.C.Y., Hager, J.W., Fang, D.-C., Cheung, A.S.-C., Chu, I.K.: Laser-induced dissociation of singly protonated peptides at 193 and 266 nm within a hybrid linear ion trap mass spectrometer. Rapid Commun. Mass Spectrom. **27**, 1119–1127 (2013)
14. Zhang, L., Reilly, J.P.: Peptide de novo sequencing using 157 nm photodissociation in a tandem time-of-flight mass spectrometer. Anal. Chem. **82**, 898–908 (2010)
15. Reilly, J.P.: Ultraviolet photofragmentation of biomolecular ions. Mass Spectrom. Rev. **28**, 425–447 (2009)

16. Brodbelt, J.S.: Photodissociation mass spectrometry: new tools for characterization of biological molecules. Chem. Soc. Rev. **43**, 2757–2783 (2014)
17. Syka, J.E.P., Coon, J.J., Schroeder, M.J., Shabanowitz, J., Hunt, D.F.: Peptide and protein sequence analysis by electron transfer dissociation mass spectrometry. Proc. Natl. Acad. Sci. U. S. A. **101**, 9528–9533 (2004)
18. Cannon, J.R., Holden, D.D., Brodbelt, J.S.: Hybridizing ultraviolet photodissociation with electron transfer dissociation for intact protein characterization. Anal. Chem. **86**, 10970–10977 (2014)
19. Shaffer, C.J., Marek, A., Pepin, R., Slováková, K., Tureček, F.: Combining UV photodissociation with electron transfer for peptide structure analysis. J. Mass Spectrom. **50**, 470–475 (2015)
20. Shaffer, C.J., Martens, J., Marek, A., Oomens, J., Tureček, F.: Photoleucine survives backbone cleavage by electron transfer dissociation. a near-UV photodissociation and infrared multiphoton dissociation action spectroscopy study. J. Am. Soc. Mass Spectrom. **27**, 1176–1185 (2016)
21. Martens, J., Grzetic, J., Berden, G., Oomens, J.: Structural identification of electron transfer dissociation products in mass spectrometry using infrared ion spectroscopy. Nat. Commun. **7**, 11754 (2016)
22. Nguyen, H.T.H., Shaffer, C.J., Tureček, F.: Probing peptide cation-radicals by near-UV photodissociation in the gas phase. structure elucidation of histidine radical chromophores formed by electron transfer reduction. J. Phys. Chem. B **119**, 3948–3961 (2015)
23. Nguyen, H.T.H., Shaffer, C.J., Ledvina, A., Coon, J.J., Tureček, F.: Serine effects on collision-induced dissociation and photodissociation of peptide cation radicals of the $z^{+\bullet}$ type. Int. J. Mass Spectrom. **378**, 20–30 (2015)
24. Shaffer, C.J., Marek, A., Nguyen, H.T.H., Tureček, F.: Combining near-UV photodissociation with electron transfer. reduction of the diazirine ring in a photomethionine-labeled peptide ion. J. Am. Soc. Mass Spectrom. **26**, 1367–1381 (2015)
25. Shaffer, C.J., Slováková, K., Tureček, F.: Near-UV photodissociation of phosphopeptide cation-radicals. Int. J. Mass Spectrom. **390**, 71–80 (2015)
26. Viglino, E., Lai, C.K., Mu, X., Chu, I.K., Tureček, F.: Ground and excited-electronic-state dissociations of hydrogen-rich and hydrogen-deficient tyrosine peptide cation radicals. J. Am. Soc. Mass Spectrom. **27**, 1454–1467 (2016)
27. Nguyen, H.T.H., Shaffer, C.J., Pepin, R., Tureček, F.: UV action spectroscopy of gas-phase peptide radicals. J. Phys. Chem. Lett. **6**, 4722–4727 (2015)
28. Viglino, E., Shaffer, C.J., Tureček, F.: UV-VIS action spectroscopy and structures of tyrosine peptide cation radicals in the gas phase. Angew. Chem. Int. Ed. **55**, 7469–7473 (2016)
29. McLuckey, S.A., Goeringer, D.E.: Slow heating methods in tandem mass spectrometry. J. Mass Spectrom. **32**, 461–474 (1997)
30. Chung, T.W., Hui, R., Ledvina, A.R., Coon, J.J., Tureček, F.: Cascade dissociations of peptide cation-radicals. part 1. scope and effects of amino acid residues in penta-, nona-, and decapeptides. J. Am. Soc. Mass Spectrom. **23**, 1336–1350 (2012)
31. Ledvina, A.R., Chung, T.W., Hui, R., Coon, J.J., Tureček, F.: Cascade dissociations of peptide cation radicals. part 2. infrared multiphoton dissociation and mechanistic studies of z ions from pentapeptides. J. Am. Soc. Mass Spectrom. **23**, 1351–1363 (2012)
32. Chu, I.K., Siu, C.-K., Lau, J.K.-C., Tang, W.K., Mu, X., Lai, C.K., Guo, X., Wang, X., Li, N., Yao, Z., Xia, Y., Kong, X., Oh, H.-B., Ryzhov, V., Tureček, F., Hopkinson, A.C., Siu, K.W.M.: Proposed nomenclature for peptide ion fragmentation. Int. J. Mass Spectrom. **390**, 24–27 (2015)
33. Holm, A.I.S., Hvelplund, P., Kadhane, U., Larsen, M.K., Liu, B., Nielsen, S.B., Panja, S., Pedersen, J.M., Skrydstrup, T., Stochkel, K., Williams, E.R., Worm, E.S.: On the mechanism of electron-capture-induced dissociation of peptide dications from 15 N-labeling and crown-ether complexation. J. Phys. Chem. A. **111**, 9641–9643 (2007)
34. Tureček, F., Julian, R.R.: Peptide radicals and cation-radicals in the gas phase. Chem. Rev. **113**, 6691–6733 (2013)
35. Roepstorff, P., Fohlman, J.: Proposal for a common nomenclature for sequence ions in mass spectra of peptides. Biomed. Mass Spectrom. **11**, 601 (1984)
36. Biemann, K.: Nomenclature for peptide fragment ions (positive ions). Methods Enzymol. **193**, 886–887 (1990)
37. Fung, Y.M.E., Chan, T.-W.D.: Experimental and theoretical investigations of the loss of amino acid side chains in electron capture dissociation. J. Am. Soc. Mass Spectrom. **16**, 1523–1535 (2005)
38. Cooper, H.J., Hudgins, R.R., Hakansson, K., Marshall, A.G.: Secondary fragmentation of linear peptides in electron capture dissociation. Int. J. Mass Spectrom. **228**, 723–728 (2003)
39. Vaisar, T., Gatlin, C.L., Rao, R.D., Seymour, J.L., Tureček, F.: Sequence information, distinction, and quantitation of C-terminal leucine and isoleucine in ternary complexes of tripeptides with Cu(II) and 2,2'-bipyridine. J. Mass Spectrom. **36**, 306–316 (2001)
40. Pepin, R., Tureček, F.: Kinetic ion thermometers for electron transfer dissociation. J. Phys. Chem. B **119**, 2818–2826 (2015)
41. Chung, T.W., Tureček, F.: Backbone and side-chain specific dissociations of *z* ions from non-tryptic peptides. J. Am. Soc. Mass Spectrom. **21**, 1279–1295 (2010)
42. Barbatti, M., Aquino, A.J.A., Lischka, H.: The UV absorption of nucleobases: semi-classical ab initio spectra simulations. Phys. Chem. Chem. Phys. **12**, 4959–4967 (2010)
43. Osburn, S., Berden, G., Oomens, J., O'Hair, R.A.J., Ryzhov, V.: Structure and reactivity of the N-acetyl-cysteine radical cation and anion: does radical migration occur? J. Am. Soc. Mass Spectrom. **22**, 1794–1803 (2011)
44. Hao, Q., Song, T., Ng, D.C.M., Quan, Q., Siu, C.K., Chu, I.K.: Arginine-facilitated isomerization: radical-induced dissociation of aliphatic radical cationic glycylarginyl(iso)leucine tripeptides. J. Phys. Chem. B **116**, 7627–7634 (2012)
45. Zhao, J., Song, T., Xu, M., Quan, Q., Siu, K.W.M., Hopkinson, A.C., Chu, I.K.: Intramolecular hydrogen atom migration along the backbone of cationic and neutral radical tripeptides and subsequent radical-induced dissociations. Phys. Chem. Chem. Phys. **14**, 8723–8731 (2012)
46. Osburn, S., Berden, G., Oomens, J., O'Hair, R.A.J., Ryzhov, V.: S-to-αC radical migration in the radical cations of Gly-Cys and Cys-Gly. J. Am. Soc. Mass Spectrom. **23**, 1019–1023 (2012)
47. Laskin, J., Kong, R.P.W., Song, T., Chu, I.K.: Effect of the basic residue on the energetics and dynamics of dissociation of phosphopeptides. Int. J. Mass Spectrom. **330–332**, 295–301 (2012)
48. Zhang, X., Julian, R.R.: Exploring radical migration pathways in peptides with positional isomers, deuterium labeling, and molecular dynamics simulations. J. Am. Soc. Mass Spectrom. **24**, 524–533 (2013)
49. Osburn, S., Berden, G., Oomens, J., Gulyuz, K., Polfer, N.C., O'Hair, R.A.J., Ryzhov, V.: Structure and reactivity of the glutathione radical cation: radical rearrangement from the cysteine sulfur to the glutamic acid α-carbon atom. ChemPlusChem. **78**, 970–978 (2013)
50. Lai, C.-K., Mu, X., Hao, Q., Hopkinson, A.C., Chu, I.K.: Formation, isomerization, and dissociation of ε- and α-carbon-centered tyrosyl glycyl glycine radical cations. Phys. Chem. Chem. Phys. **16**, 24235–24243 (2014)
51. Xu, M., Tang, W.-K., Mu, X., Ling, Y., Siu, C.-K., Chu, I.K.: α-Radical-induced CO_2 loss from the aspartic acid side chain of the collisionally induced tripeptide aspartylglycylarginine radical cation. Int. J. Mass Spectrom. **390**, 56–62 (2015)
52. Lesslie, M., Osburn, S., van Stipdonk, M.J., Ryzhov, V.: Gas-phase tyrosine-to-cysteine radical migration in model systems. Eur. J. Mass Spectrom. **21**, 589–597 (2015)
53. Osburn, S., Chan, B., Ryzhov, V., Radom, L., O'Hair, R.A.J.: Role of hydrogen bonding on the reactivity of thiyl radicals: a mass spectrometric and computational study using the distonic radical ion approach. J. Phys. Chem. A **120**, 8184–8189 (2016)
54. Mayer, J.M.: Proton-coupled electron transfer: a reaction chemist's view. Ann. Rev. Phys. Chem. **55**, 363–390 (2004)
55. Warren, J.J., Tronic, T.A., Mayer, J.M.: Thermochemistry of proton-coupled electron transfer reagents and its implications. Chem. Rev. **110**, 6961–7001 (2010)
56. Cox, K.A., Gaskell, S.J., Morris, M., Whiting, A.: Role of the site of protonation in the low-energy decompositions of gas-phase peptide ions. J. Am. Soc. Mass Spectrom. **7**, 522–531 (1996)
57. Jones, J.L., Dongre, A.R., Somogyi, A., Wysocki, V.H.: Sequence dependence of peptide fragmentation efficiency curves determined by electrospray ionization/surface-induced dissociation mass spectrometry. J. Am. Chem. Soc. **116**, 8368–8369 (1994)
58. Paizs, B., Suhai, S.: Fragmentation pathways of protonated peptides. Mass Spectrom. Rev. **24**, 508–548 (2005)